Journal of Magnetic Resonance 194 (2008) 33–40

Contents lists available at ScienceDirect

Journal of Magnetic Resonance

journal homepage: www.elsevier.com/locate/jmr

The dependence on magnetic field strength of correlated internal gradient relaxation time distributions in heterogeneous materials

K.E. Washburn [a], C.D. Eccles [b], P.T. Callaghan [a,*]

[a] School of Chemical and Physical Sciences, Victoria University of Wellington, P.O. Box 600, Wellington 6001, New Zealand
[b] Magritek Limited, Wellington, New Zealand

ARTICLE INFO

Article history:
Received 30 March 2008
Revised 20 May 2008
Available online 4 June 2008

Keywords:
Internal gradients
Field dependence
Porous media

ABSTRACT

Magnetic susceptibility differences in porous media produce local gradients within the pore space. At high magnetic fields, these inhomogeneities have the potential to greatly affect nuclear magnetic resonance measurements. We undertake a study using a new NMR technique to measure the internal gradients present in highly heterogeneous samples over a wide range of magnetic field strengths. Our results show that even at ultra-high fields there can exist signal at internal gradient strengths sufficiently small that techniques for suppressing unwanted side effects have the possibility to be used. Our findings encourage the use of these high and ultra-high field strengths for a broader range of samples. Our results also give experimental evidence to support the theory of internal gradient scaling as a function of field strength within pores.

1. Introduction

Nuclear magnetic resonance (NMR) experiments on heterogenous porous media are often performed at low magnetic fields [1–8], with proton Larmor frequencies on the order of a few megahertz. Even at these low fields, the heterogeneous nature of the samples has the potential to broaden the spectrum for NMR measurements. When there exists a magnetic susceptibility difference between materials in a sample, for example between a porous matrix and a saturating fluid, local magnetic field gradients develop at the interfaces. The inhomogeneities in the local magnetic field lead to spatial variations referred to as "internal gradients". The main factors governing the strength of these gradients depend on the susceptibility difference between the materials, the applied magnetic field, and the pore size, though grain size, pore shape, and the geometry of the pore network also have an influence. The internal gradients intensities are roughly inversely proportional with pore size and scale linearly with applied field strength as

$$g \sim \Delta\chi B_0 \tag{1}$$

where g is the local magnetic field gradient experienced by the spins, $\Delta\chi$ is the magnetic susceptibility difference between the fluid and pore surface, and B_0 is the applied magnetic field. The internal gradients can interfere with NMR measurements in a variety of ways. The inhomogeneities cause a broadening of the linewidths in chemical spectra. The interaction between the internal gradients and applied field gradients can produce distorted images and inaccurate diffusion measurements. The internal gradients can introduce a bias in transverse relaxation and diffusion measurements due to extra dephasing of the signal.

NMR research in heterogeneous materials has not been limited to low field [9–13], as increased field strength confers advantages, such as higher signal to noise, small sample requirements, and long relaxation times. With their dependence on field strength, these internal gradients become more prominent at higher magnetic fields. What may have been a negligible effect at low field often becomes a serious concern at high field and many techniques have been developed to deal with the unwanted side effects of internal gradients. The line broadening caused by the internal gradients can make identification of chemical shifted components in the spectral dimension impossible. de Swiet et al. [14] have tried to overcome this using magic angle spinning while Seland et al. [15] used diffusion attenuation. Cotts et al. [16], Sorland et al. [17,19], and Sun [18] have developed bipolar gradient sequences to compensate for interactions between the applied and internal gradients in diffusion experiments.

Despite their potential to distort experiments, the internal gradients within a sample are not always a nuisance. Because of their dependence on characteristics of the pore space, several techniques have been developed to take advantage of internal gradients to find pore shape [20], pore connectivity, [21] or wettability [22]. We present here a novel 2D inverse Laplace NMR technique which could assist better understanding of the distribution of internal gradients as a function of pore size. This method correlates internal gradients with T_1 relaxation, the time the excited spins take to return to equilibrium

* Corresponding author. Fax: +64 6 350 5164.
E-mail address: Paul.Callaghan@vuw.ac.nz (P.T. Callaghan).

1090-7807/$ - see front matter © 2008 Elsevier Inc. All rights reserved.
doi:10.1016/j.jmr.2008.05.025

with their environment. By contrast with the measurement of T_2 or the restricted diffusion coefficient, measurement of T_1 relaxation is not susceptible to the presence of internal gradients. This makes it ideal for use at high and ultra-high fields where internal gradients could potentially be significant. We also undertake the first experimental study of how internal gradients in differing pore sizes scale as a function of applied field.

2. Theory

Internal magnetic field gradients affect transverse magnetisation by enhancing the loss of spin coherence as spin-bearing molecules diffuse through the inhomogeneities. The additional decoherence produces attenuation in the measured signal, leading to a potential bias in the T_2 measurement. Were the spin-bearing molecules to remain stationary, the local magnetic fields would remain constant and the decoherence which arises from the distribution of local fields could be reversed by the spin-echo process. However, these molecules diffuse in the case of liquids imbibed in porous media. This has the effect that the magnetic fields experienced by the spins are time varying, leading to a subtle motional averaging process in the evolving phases of the the ensemble of spins. To understand this process it is helpful to define a length scale l_g over which a molecule must diffuse for significant irreversible dephasing to occur. This length is defined by [23]

$$l_g = \left(\frac{D_0}{\gamma g}\right)^{\frac{1}{3}}, \tag{2}$$

where D_0 is the diffusion coefficient of the fluid and γ is the gyromagnetic ratio. Of course, in a porous medium, that gradient will change, typically over distances on the length scale of structural features. That point we will address.

In order to ensure that diffusive attenuation of the spin-echo signal is minimised, the Carr–Purcell–Meiboom–Gill 180° rf pulse train is used. For a CPMG pulse sequence with echo spacing t_E, the distance traveled between echoes is on the order of $l_E = (D_0 t_E)^{\frac{1}{2}}$. Provided $l_E \ll l_g$, the echo attenuation between successive pairs of echoes is small, and the cumulative attenuation over many echoes is the result of successively small dephasing. For the experiments performed here, in which variable echo spacings are used, the observation of a signal after several echoes requires that the condition $l_E \ll l_g$ is satisfied for all measurements. The size of the local gradient can readily be seen by changing the echo spacing of a Carr–Purcell–Meiboom–Gill (CPMG) [24,25] train. As the echo spacing is increased, the apparent dephasing rate of the spins increases. This increased relaxation rate arises from diffusion through the internal gradients while the relaxation due to T_2 remains constant [5].

While absolute gradients scale linearly with the applied field strength as $\Delta\chi B_0$, it may be shown that there is an upper limit to the effective gradient which can be measured, namely when the structural features have length scales on the order of l_g. These maximum possible measured gradients within a sample are given by the relation [23]:

$$g_{max} \approx \left(\frac{\gamma}{D_0}\right)^{\frac{1}{2}} (\Delta\chi B_0)^{\frac{3}{2}} \tag{3}$$

while the associated structural length scale is given by l_s. There is a critical length of l_s, defined as

$$l^* = \left(\frac{D_0}{\gamma \Delta\chi B_0}\right)^{\frac{1}{2}}. \tag{4}$$

For pores smaller than l^*, the fluctuations in gradient as molecules diffuse means that the local gradients are averaged over the dephasing length. As l_s begins to approach l^*, the measured effective gradient begins to approach g_{max}. For pores larger than l^*, the dephasing of the CPMG echo signal which occurs over the echo time t_E, such that $l_E \ll l_s$, arises from a local gradient which is effectively constant. Hence, the overall echo train attenuation may be calculated by averaging over the distribution of gradients in the ensemble of spins.

The technique for measurement of internal gradients is a modified CPMG sequence that capitalises [26] upon the changing echo amplitude as a function of echo spacing. We take a constant interval of time, t_0, and vary the number of 180° pulses, which refocus the magnetisation. Thus, the echo spacing t_E for an individual experiment is

$$t_E = 2\tau_n = \frac{t_0}{n}, \tag{5}$$

where n is the number of 180° pulses in the time period. As we increase the number of pulses in this time period, the spin-bearing molecules have less time to diffuse through the internal gradients, lessening the dephasing effect. In some situations, below a certain τ_n, the intensity of the measured echo will plateau. For these cases, the echo spacing is sufficiently short that the influence of internal gradients upon the signal has become negligible.

In the "local gradient" regime, the echo amplitude of a CPMG echo train in the presence of internal gradients is described by:

$$\begin{aligned}\frac{M(t_i)}{M_0} &= \sum_j f_j \exp\left[-\frac{t_i}{T_{2j}}\right] \int_j P_j(g) \exp\left[-\frac{\gamma^2 g^2 \tau_n^2 D t_i}{3}\right] dg \\ &= \sum_j f_j \exp\left[-\frac{t_i}{T_{2j}}\right] \int_j P_j(g) \exp\left[-\frac{\gamma^2 g^2 t_0^2 D t_i}{12 n^2}\right] dg \end{aligned} \tag{6}$$

where M_0 is the initial signal intensity, f_j is the volume fraction of pore sizes that produce a transverse relaxation time T_{2j}, $P_j(g)$ is the volume fraction of pore sizes that produce an internal gradient of magnitude g, τ_n is the echo spacing and t_i the echo train time. Note that this relation only holds true in the local gradient regime; the transverse relaxation decay in the motional averaging regime loses the dependence on the CPMG echo spacing.

Only in the rare situation of a monodisperse pore space can the magnitude of internal gradients be found uniquely. For polydisperse porous materials, the internal gradients are coupled to pore size, and the internal gradient values will be widely dispersed. To separate different gradient components, the multiexponential decay can be analysed using 1D inverse Laplace methods. An even more effective separation results if the gradient can be correlated with another parameters also dependent on pore size and a 2D inversion performed. One approach followed by Sun and Dunn [26] is to use T_2 relaxation to decouple the internal gradients from pore size. Instead, we choose to use the T_1 times of a system, which are related to pore size as:

$$\frac{1}{T_1} = \frac{1}{T_{1Bulk}} + \rho_1 \frac{S}{V}, \tag{7}$$

where T_{1Bulk} is the T_1 relaxation time of the bulk fluid, ρ_1 is the surface relaxivity of the system, S is the pore surface area and V is the pore volume. Both the values of T_{1bulk} and ρ_1 are frequency dependent. T_{1bulk} increases as a function of field strength while ρ_1 decreases.

Fig. 3 shows a pulse sequence in which both T_1 relaxation and the external gradient dephasing effects are correlated. The signal attenuation for this pulse sequence is given by:

$$\begin{aligned} M(\tau_{T1}, \tau_n) = \Sigma_j f_j^0 & \\ & \times \exp\left(\frac{-t_0}{T_{2j}}\right) \int\int F_j(T_1, g) \left(1 - 2\exp\left[-\frac{\tau_{T1j}}{T_1}\right]\right) \\ & \times \exp\left[-\frac{\gamma^2 g^2 \tau_n^2 D t_0}{3}\right] dT_1 dg + \epsilon(\tau_{T1}, \tau_n) \end{aligned} \tag{8}$$

where $F_j(T_1,g)$ is the joint probability density and ϵ is the experimental noise. Precise 180° pulses are important to obtaining the true T_1 distribution and our 180° pulses were found using the standard technique of measuring a range of rf pulse durations to find the one which will produce a signal null. We can treat the T_2 relaxation during the internal gradient interval, t_0, as a constant and ignore it in the inversion calculations as it will be the same for all experiments at different τ_n and constant t_0. It will therefore result in a fixed intensity weighting for each T_{2j}. Similarly, the amount of T_1 relaxation that occurs during the internal gradient encoding interval can be ignored provided that the 180° rf pulses are sufficiently accurate. This requires both high rf bandwidth (to cover the linewidth) and good homogeneity. The latter is never perfect but the phase cycling effect of the CPMG train compensates for that. In our experiments the rf pulses are sufficiently short that the bandwidth requirements are met. Finally we point out that because the CPMG train covers a fixed interval, t_0, any residual T_1 relaxation should, as is the case for T_2, constitute a fixed additional intensity weighting for each peak. However, the effect of T_2 cannot be ignored as a whole in the experiment. The 180° pulses serve to correct for the reversible spin decoherence caused by the local inhomogeneities, but the underlying irreversible spin–spin relaxation is unaffected. Therefore, any signal which has a T_2 time shorter than the internal gradient interval will decay away and not appear in the $T_1 - g$ plot. In addition, while the T_2 relaxation will not affect the peak locations in our experiment, it will influence the intensity of the peaks. If quantification of the spectra are to be performed, the intensity should be corrected using $T_1 - T_2$ and $T_2 - g$ correlation experiments.

3. Experimental

The experiments were performed on a Magritek 12 MHz Kea and Bruker 200 MHz Avance, 400 MHz Avance II and 900 MHz Avance II+ Spectrometers. Two samples were used: Mt. Gambier limestone and tight packed New Zealand quartz beach sand. X-ray CT images of the samples shown in Figs. 1 and 2. The samples were saturated with distilled water before experimentation and held at a constant temperature of 25 °C for the duration of the experiments. Using the inhomogeneous linewidth, we calculated the magnetic susceptibility differences for the New Zealand quartz beach sand and Mt. Gambier limestone to be $\Delta\chi = 30 \times 10^{-6}$ and $\Delta\chi = 9 \times 10^{-6}$, respectively. This technique compares the linewidth

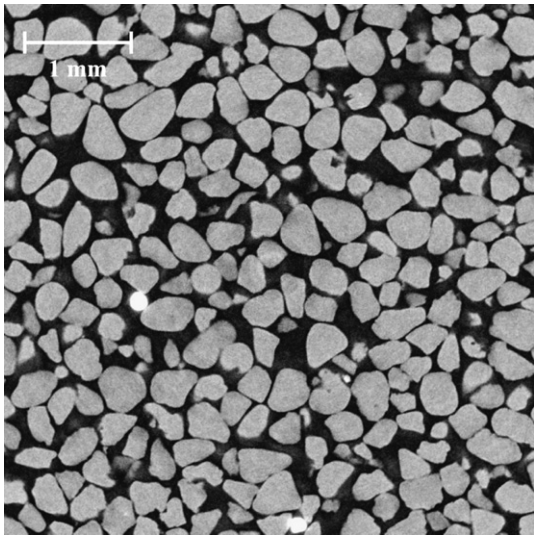

Fig. 1. X-ray CT of tight packed quartz sand.

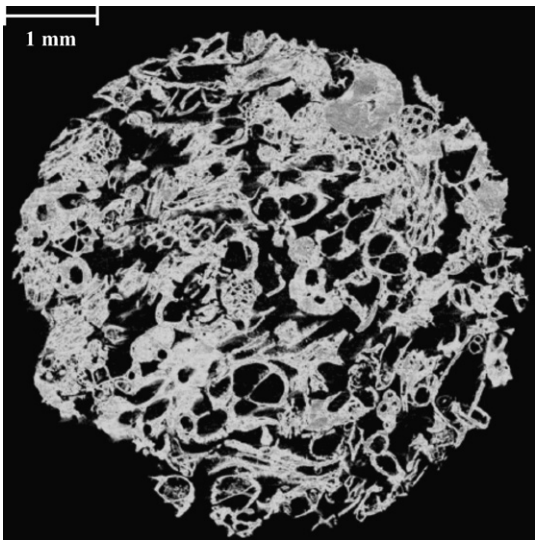

Fig. 2. X-ray CT of Mt. Gambier limestone.

of the Fourier transformed spectra of a bulk fluid and the fluid imbibed in a material. The broadening in the linewidth can be related to the magnetic susceptibility difference as [28]

$$\Delta\nu \approx \frac{\gamma\Delta\chi B_0}{2\pi}. \tag{9}$$

We used these values to determine the critical length l^*, shown Table 1.

As the majority of the pores in both the sand and Mt. Gambier samples are larger than our calculated critical lengths, we believe we can reliably apply the local field gradient assumption and assume free diffusion through the internal gradients for all field strengths.

Fig. 3 shows the pulse sequence. The T_1 encoding was performed in 30 steps, ranging from a τ_{T1} of 1–1500 ms. For the internal gradient encoding, the length of the t_0 intervals were 60, 40, 32 and 19.2 ms at 12, 200, 400 and 900 MHz, respectively. The length of this interval is the time necessary for the measured echo of the longest echo spacing to be completely attenuated. There were 40 steps for internal gradient encoding, with the number of refocusing 180° pulses ranging from 1 to 400. The number of refocusing pulses was selected so that the echo intensities reached a plateau for the shortest values of τ_n. The data were Fourier transformed along the acquisition dimension and the resulting peak was integrated,

Table 1
Calculated critical lengths l^*

Sample (MHz)	Mt. Gambier (μm)	Quartz sand (μm)
12	0.4	0.3
200	0.1	0.06
400	0.08	0.04
900	0.05	0.03

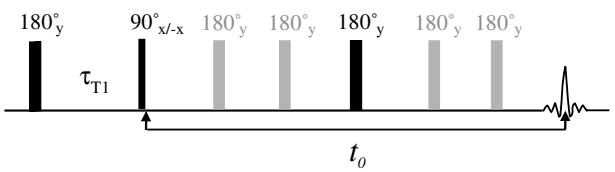

Fig. 3. Pulse sequence for the $T_1 - g$ experiment.

producing a 2D plot of τ_{T_1} versus t_n in the time dimension. A 2D inverse Laplace transform [29] was applied to the spectrum to give a 40×30 matrix. The α value chosen for regularisation of the inverse Laplace transform minimised the value of χ^2 and no further. Because the experiments measure the internal gradients as a function of diffusion, we then use the diffusion coefficient of 2.3×10^{-5} cm/s for water at room temperature. We assume we are in the free diffusion limit for the internal gradient interval, as the molecules will only diffuse 5–10 μm during that time, which is less than the pore size for most pores in the samples.

4. Results and discussion

Figs. 4 and 5 show the measured $T_1 - g$ plots for the quartz sand and Mt. Gambier samples as a function of the different field strengths. Fig. 6 gives an expanded view of the $T_1 - g$ plots for the two samples at 12 and 900 MHz so the details of difference in the T_1 resolution with field strength can be seen. Figs. 7 and 8. shows the projected 1D plots of the internal gradient dimension from the $T_1 - g$ plots, which highlights the advantage of having the T_1 dimension to add resolution to the spectra. A direct 1D transform upon the internal gradient data alone allows even less detail in the spectra to be resolved.

Surprisingly, even at the ultra-high field of 900 MHz there exists signal at relatively low internal gradients. The maximum measured gradients are on the order of $\sim 10^5$ G/cm. We note that relation $l_E \ll l_g$ holds true even for these high internal gradient strengths. The largest measured internal gradients are calculated using only the very early decay of the CPMG, for which τ_n is short and hence the condition $l_E \ll l_g$ is still satisfied. An advantage of the 2D $T_1 - g$ correlation is that it gives better resolution, allowing us to discern subtle details in the spectra. At higher field strengths in the $T_1 - g$ plots, we see several distinct regions of T_1, whereas a 1D inversion only gives a singular broad distribution. For 200 MHz and above field strengths, we see a clear negative correlation between T_1 and internal gradient strength. This reflects with expected behaviour as larger pores will produce longer T_1 values and weaker internal gradients while smaller pores will produce shorter T_1 values and stronger internal gradients.

For the most part, the distribution of internal gradients stays the same for the different magnetic field strengths. This indicates that signal measured at the higher applied fields is still mostly representative of the pore space. The results of Winkler et al. [30] raised a concern that the measured signal at high magnetic fields might come from only a small fraction of the fluid present. However, in the Mt. Gambier sample, the peak of highest intensity at low field strength disappears at the higher fields. We believe the peak has moved to internal gradient strengths higher than we can currently measure due to machine limitations, so it appears some loss of signal does occur at higher applied fields. When we attempted to move to shorter echo spacings at 200 and 400 MHz, we sometimes encountered problems exceeding the duty cycle of the spectrometers, causing the transmitter to shut down. At 900 MHz, the transmitter of the newer spectrometer was able to handle the demand of shorter echo spacings, but the system was fitted with a cryoprobe for high resolution spectroscopy. These are not as robust as normal probes and the shorter echo spacings caused excessive heating in the cryoprobe, making it unwise to continue. Therefore, at higher applied magnetic fields one must be aware that signal loss from internal gradients may occur, particularly with older equipment.

For internal gradient measurements, working at high field may actually enable us to probe a greater proportion of the pore space as the value of l^* becomes smaller with increased field. While incomplete sampling of the pore space is not an concern for the samples used here, this could potentially be an issue for samples with lower magnetic susceptibility differences. For example, mudstones often have low magnetic susceptibility differences. As the pore sizes can be extremely small in mudstones, the internal gra-

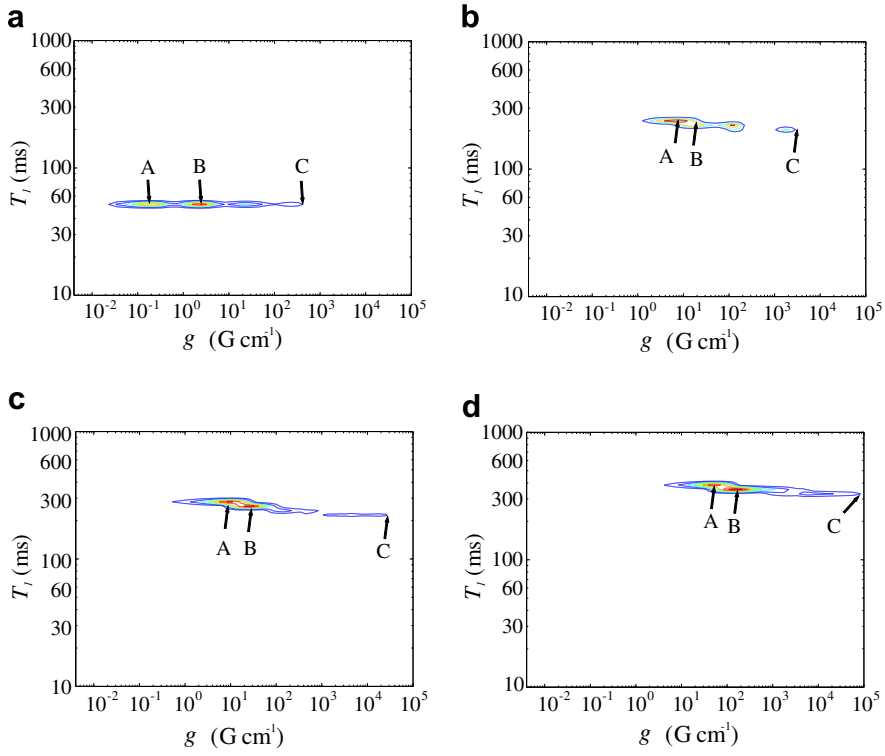

Fig. 4. $T_1 - g$ plots for the tight packed quartz sand at (a) 12 MHz, (b) 200 MHz, (c) 400 MHz, and (d) 900 MHz. *A*, *B*, and *C* arrows indicate the tracked intensity.

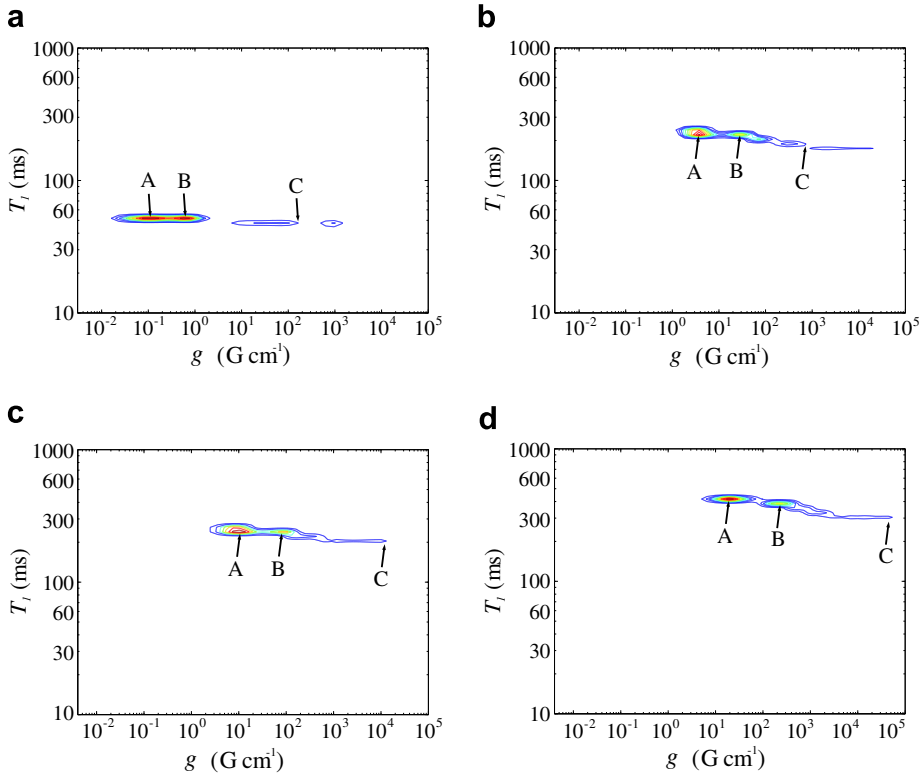

Fig. 5. $T_1 - g$ plots for the Mt. Gambier limestone at (a) 12 MHz, (b) 200 MHz, (c) 400 MHz, and (d) 900 MHz. *A*, *B*, and *C* arrows indicate the tracked intensity.

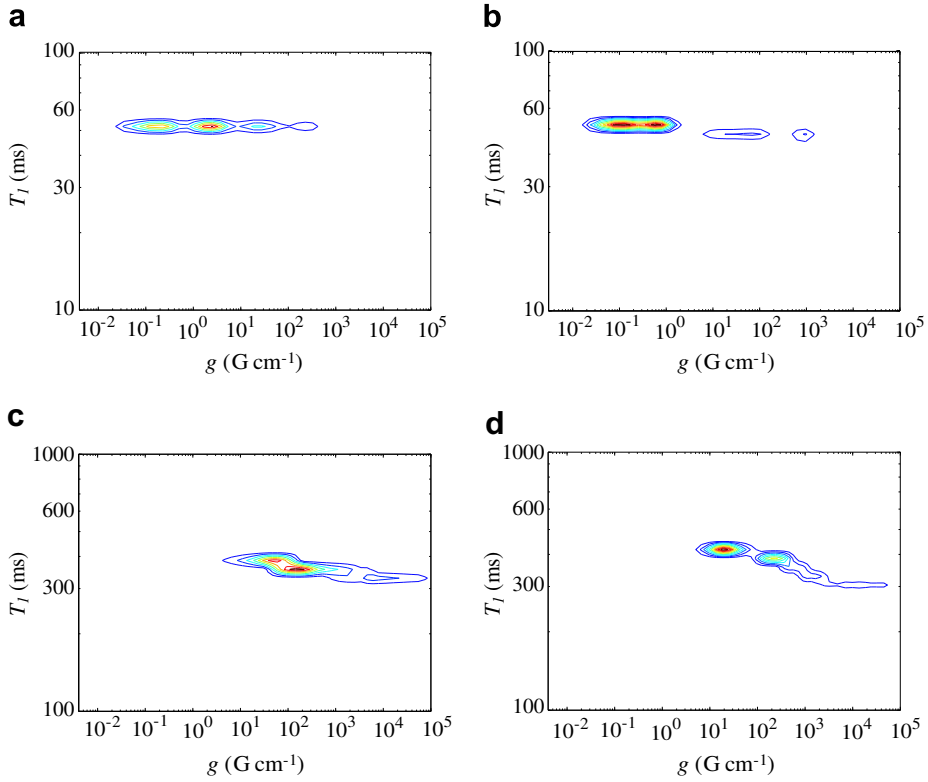

Fig. 6. $T_1 - g$ plots for the (a) quartz sand at 12 MHz, (b) Mt. Gambier limestone at 12 MHz, (c) quartz sand at 900 MHz, and (d) Mt. Gambier limestone at 900 MHz.

dients for a significant portion of the pore space would be unable to be probed at low field. However, for the CPMG decay to be affected by internal gradients, l_E must be less than l^* to encode for these pores. This is usually not a concern with modern equipment, but can become a problem with the duty cycle for older spectrometers.

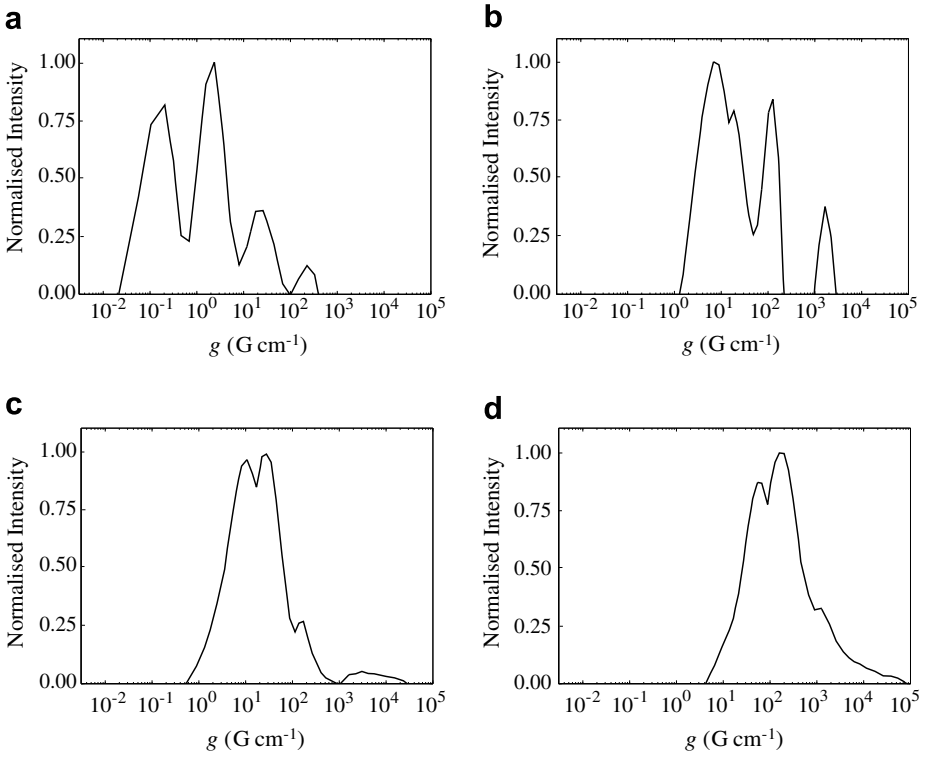

Fig. 7. 1D project of the internal gradient dimension in quartz sand at (a) 12 MHz, (b) 200 MHz, (c) 400 MHz, and (d) 900 MHz.

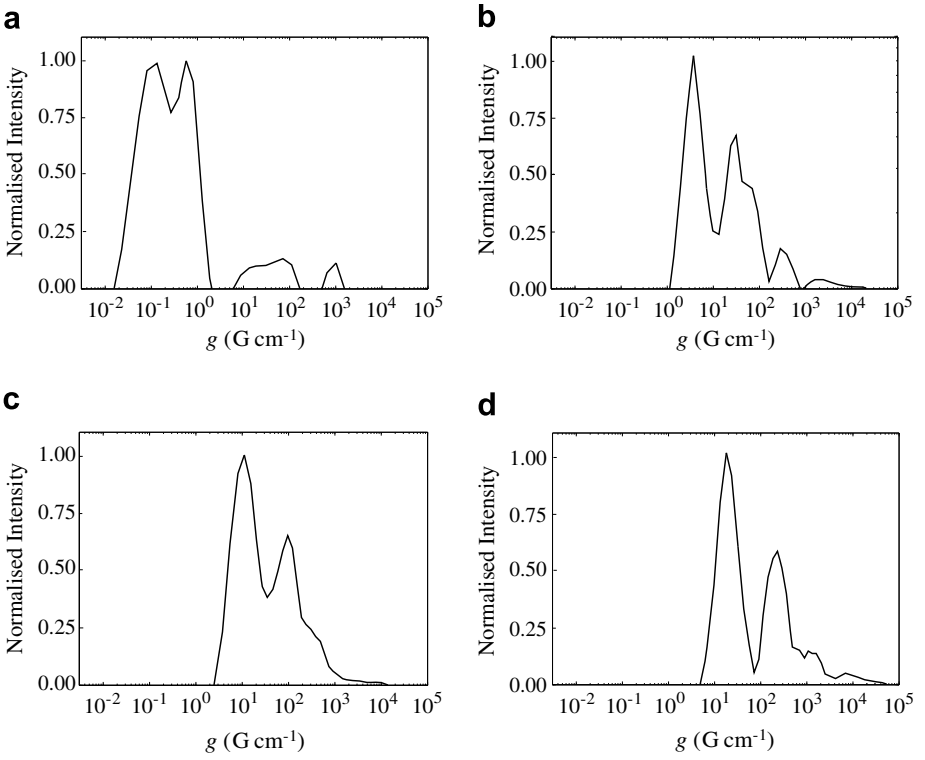

Fig. 8. 1D project of the internal gradient dimension in Mt. Gambier limestone at (a) 12 MHz, (b) 200 MHz, (c) 400 MHz, and (d) 900 MHz.

Using our estimated susceptibility differences and Eq. (3), we calculate the expected maximum gradients present in the samples and compare them to the maximum gradients present in the inverted spectra, shown Tables 2 and 3. For the Mt. Gambier, the maximum measured gradients for 400 and 900 MHz agree well with calculations. At the lower field strengths, there is a measured peak found at gradients higher than the calculated values. This may arise from an area of paramagnetic impurity in the sample which has a higher than average $\Delta\chi$. If we ignore this anomalously high gradient peak, our measured values at these field strengths

Table 2
Maximum calculated gradients (G/cm^{-1})

Sample (MHz)	Mt. Gambier	Quartz sand
12	$10^{1.8}$	$10^{2.5}$
200	$10^{3.6}$	$10^{4.3}$
400	$10^{4.1}$	$10^{4.8}$
900	$10^{4.5}$	$10^{5.3}$

Table 3
Maximum measured gradients (G/cm^{-1})

Sample (MHz)	Mt. Gambier	Quartz sand
12	$10^{3.0}$	$10^{2.3}$
200	$10^{4.1}$	$10^{3.9}$
400	$10^{4.1}$	$10^{4.3}$
900	$10^{4.5}$	$10^{4.8}$

agree better with theory. The sand sample follows the general trend, but consistently has slightly lower measured values than the calculated maximum gradients. It is possible that a higher gradient signal component exists at these internal gradient strengths, but at such a low intensity compared to the other signal present that they are below the resolution threshold on the inverse Laplace transform. For the low field, the T_1 times for the different internal gradient strengths are nearly the same. As we increase field strength, we begin to see better distinction of the peaks in the T_1 dimension, highlighting better resolution in the T_1 domain as an advantage of working at higher magnetic fields in these samples. However, as we increase field strength, we seem to lose some resolution in the internal gradient dimension, particularly in the sand sample.

We now consider how the internal gradients and T_1 relaxation times scale as a function of B_0 for both the sand and Mt. Gambier samples. In our spectra, we see several distinct regions of intensities which reflect different sizes in the pore space within the sample. To aid in tracking the signal between field strengths, we assign letters to different regions of the signal. The signal components arising from larger pores in the samples, identified as *A* and *B*, are easy to track because of distinctive peaks. Unfortunately, with the smaller pores at higher applied fields, we lose distinguishing peaks, so we simply choose to follow the maximum measured intensity for each spectrum, which we label *C*. For consistency with the Mt. Gambier sample, we track the maximum intensity for the second highest peak at 12 and 200 MHz due to the loss of the highest gradient peak at higher field strengths. Error bars were calculated using the peak locations from repeated measurements.

Internal gradients strengths as a function of field strength are shown in Fig. 9 with the best fit lines shown in Table 4. For both *A* and *B* peaks the magnetic field scaling is approximately unity. For the *C* peak the internal gradients scale as a function of $B_0^{1.3}$. These results agree well with the theory put forth by Hürlimann; the larger pores scale as approximately B_0 whereas the maximum observable gradients, corresponding to small pores approaching l^*, scale at up to $B_0^{1.5}$. For the smaller pores where $l_s < l^*$, the local gradients will be averaged out by diffusion. If $l_s = l^*$, the strength of the gradient is such that diffusion can no longer average the local gradient of the pore and the effective gradients can approach the limit of $B_0^{\frac{3}{2}}$.

Table 4
Scaling factors

Mt. Gambier	g	T_1	Quartz sand	g	T_1
A	$B^{1.1}$	$B^{0.49}$	*A*	$B^{1.1}$	$B^{0.48}$
B	$B^{1.1}$	$B^{0.47}$	*B*	$B^{1.0}$	$B^{0.48}$
C	$B^{1.3}$	$B^{0.42}$	*C*	$B^{1.3}$	$B^{0.42}$

Fig. 10 shows T_1 as a function of field strength with the best fit lines shown in Table 4. The T_1 values of the *A* and *B* peaks scale as a function of $B_0^{0.5}$, which agrees with the T_1 frequency dependence of $T_1 \propto \omega^{0.5}$ in water saturated porous media seen by Korb et al. [27]. For the *C* limit, T_1 scales only as $B_0^{0.4}$. While surface relaxation is known to decrease with increased field strength, cursory examination of Eq. (7) shows that as the T_1 of the saturating fluid increases with field strength, a broader distribution of T_1 values will be produced from the surface relaxivity for a given pore size distribution. This explains the increase in resolution we see in the T_1 domain. Because of this scaling, nearly an order of magnitude in T_1 relaxation time is gained between the low field and the high field experiments. The increased T_1 relaxation time is a particular advantage for exchange experiments [32,31,13]. With proper bipolar gradients and sufficiently short echo times [16], diffusion exchange and transverse relaxation exchange experiments can take advantage of the long T_1 times to increase the mixing times, which allows longer length scales within the material to be probed without sacrificing the reliability of the measurements.

5. Conclusion

We provide experimental evidence that the effective internal gradients present in a sample can scale as B_0 while maximum observable gradients can scale at up to $B_0^{\frac{3}{2}}$. Our results show that it is possible to reliably perform experiments on even highly heterogeneous samples at high fields and that advantages come at these high fields. For these samples, the $T_1 - g$ correlation is a useful initial experiment to estimate the expected internal gradients. The large internal gradients that arise at high field can be accessed through short echo spacing and those that are too high given the shortest experimentally available t_E will not contribute to the mea-

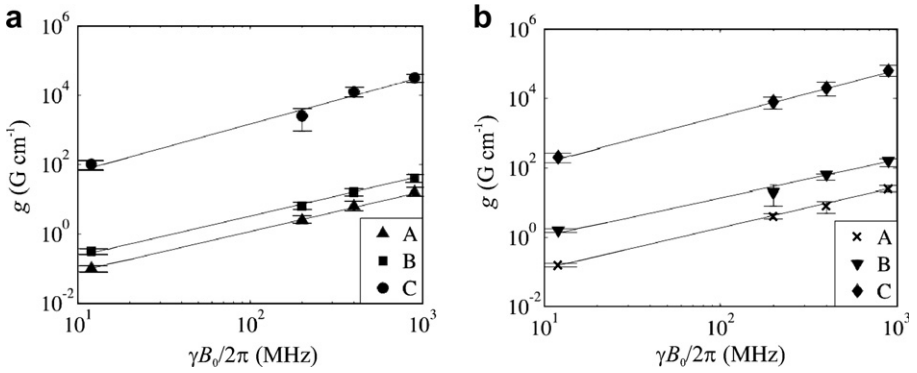

Fig. 9. Internal gradient magnitude as a function of field strength for (a) Mt. Gambier and (b) quartz sand with best fit lines.

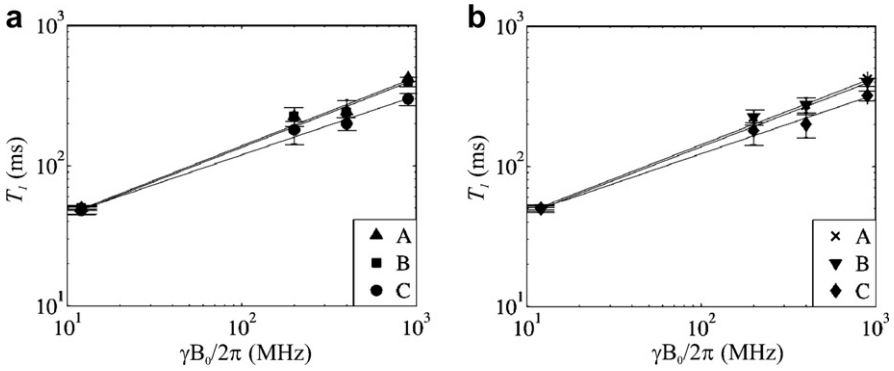

Fig. 10. T_1 relaxation time as a function of field strength for (a) Mt. Gambier and (b) quartz sand with best fit lines.

sured signal. We find evidence that there is some signal loss at high applied fields. Here, one must bear in mind, that the 900 MHz data may possibly not represent a complete picture of the system. We anticipate as spectrometer technology improves, we will be able to measure the higher gradients in the sample even at the highest fields, helping to rectify this loss of signal. Interesting future work could combine our technique with the MAS techniques [14] developed for internal gradient suppression. Our findings certainly encourage the use of these high and ultra-high field strengths for a broader range of samples.

Acknowledgments

The authors acknowledge the Royal Society of New Zealand Marsden fund for financial support. The authors thank G. Pierens and S.J. Hill for help in performing the experiments on the 200 and 900 MHz systems, E. Ryeng for formatting help, and E. Anderssen for discussion. The authors also thank C.H. Arns for the X-ray CT images.

References

[1] P.M. Singer, G. Leu, E.J. Fordham, P.N. Sen, Low magnetic fields for flow propagators in permeable rocks, J. Magn. Reson. 183 (2006) 167.
[2] J. Arnold, C. Clauser, R. Peching, S. Anferova, V. Anferon, B. Bluemich, Porosity and permeability from mobile NMR core-scanning, Petrophysics 47 (2006) 306 .
[3] R.C. Wilson, M.D. Hurlimann, T_1/T_2 ratio and frequency dependence of NMR relaxation in porous sedimentary rocks, J. Magn. Reson. 183 (2006) 1.
[4] G.H. Sorland, H.W. Anthonsen, J.G. Seland, F. Antonsen, H.C. Wideroe, J. Krane, Exploring the separate NMR responses from crude oil and water in rock cores, Appl. Magn. Reson. 26 (2004) 417.
[5] R.L. Kleinberg, S.A. Farooqui, M.A. Horsfield, Transverse relaxation processes in porous sedimentary rock, J. Col. Inter. 158 (1993) 195 .
[6] C.H. van der Zwaag, E. Veliyulin, T. Skjetne, A.E. Lothe, R.M. Holt, O.M. Nes, Deformation and failure of rock samples probed by T1 and T2 relaxation, Magn. Reson. Imaging 21 (2003) 405.
[7] P.J. McDonald, J.P. Korb, J. Mitchell, L. Monteilhet, Surface relaxation and chemical exchange in hydrating cement pastes: a two-dimensional NMR relaxation study, Phys. Rev. E 72 (2005) 011409.
[8] C. Casieri, F. De Luca, P. Fantazzini, Pore-size evaluation by single-sided nuclear magnetic resonance measurements: compensation of water self-diffusion on transverse relaxation, J. Appl. Phys. 97 (2005) 011409.
[9] D.J. Holland, U.M. Scheven, P.J. Middelberg, L.F. Gladden, Quantifying transport within a porous medium over a hierarchy of length scales, Phys. Fluids 18 (2006) 033102.
[10] M.L. Johns, A.J. Sederman, L.F. Gladden, A. Wilson, S. Davies, Using MR techniques to probe permeability reduction in rock cores, AIChE 49 (2004) 1076.
[11] F. Stallman, C. Vogt, J. Karger, K. Helbig, F. Jacobs, Aging and non linear rheology in suspensions of PEO-protected silica particles, J. Chem. Phys. 119 (2003) 9609.
[12] Q. Chen, A.E. Marble, B.G. Colpitts, B.J. Balcom, The internal magnetic field distribution and single exponential magnetic resonance free induction decay in rocks, J. Magn. Reson. 175 (2005) 300.
[13] K.E. Washburn, P.T. Callaghan, Tracking pore to pore exchange using relaxation exchange spectroscopy, Phys. Rev. Lett. 97 (2006) 175502.
[14] D. de Swiet, M. Tomaselli, M.D. Hurlimann, A. Pines, In situ NMR analysis of fluids contained in sedimentary rock, J. Magn. Reson. 133 (1998) 385.
[15] J.G. Seland, G.H. Sorland, H.W. Anthonsen, J. Krane, Combining PFG and CPMG NMR measurements for separate characterization of oil and water simultaneously present in a heterogeneous system, Appl. Magn. Reson. 24 (2003) 41.
[16] R. Cotts, M. Hoch, T. Sun, J. Markert, Pulsed field gradient simulated echo methods for improved NMR diffusion measurements in heterogeneous systems, J. Magn. Reson. 83 (1989) 252.
[17] G.H. Sorland, D. Aksnes, L. Gjerdaker, A pulsed field gradient spin-echo method for diffusion measurements in the presence of internal gradients, J. Magn. Reson. 137 (1999) 397.
[18] P.Z. Sun, Improved diffusion measurement in heterogeneous systems using the magic asymmetric gradient stimulated echo (MAGSTE) technique, J. Magn. Reson. 187 (2007) 77.
[19] G.H. Sorland, J.G. Seland, J. Krane, H.W. Anthonsen, Improved convection compensating pulsed field gradient spin-echo and stimulated-echo methods, J. Magn. Reson. 142 (2000) 323.
[20] Q. Chen, Y.Q. Song, What is the shape of pores in natural rocks?, J Chem. Phys. 116 (2002) 8247.
[21] Y.Q. Song, S. Ryu, P. Sen, Determining multiple length scales in rocks, Nature 406 (2000) 178.
[22] J.G. Seland, K.E. Washburn, H.W. Anthonsen, J. Krane, Correlations between diffusion, internal magnetic field gradients, and transverse relaxation in porous systems containing oil and water, Phys. Rev. E 70 (2004) 051305.
[23] M.D. Hurlimann, Effective gradients in porous media due to susceptibility differences, J. Magn. Reson. 131 (1998) 232.
[24] H.Y. Carr, E.M. Purcell, Effects of diffusion on free precession in nuclear magnetic resonance experiments, Phys. Rev. 94 (1954) 630.
[25] S. Meiboom, D. Gill, Modified spin-echo method for measuring nuclear relaxation times, Rev. Sci. 29 (1958) 688.
[26] B.Q. Sun, G. Dunn, Probing the internal field gradients of porous media, Phys. Rev. E 65 (2002) 051309.
[27] J.P. Korb, M.W. Hodges, T.H. Gobron, R.G. Bryant, Anomylous surface diffusion of water compared to aprotic liquids in nanopores, Phys. Rev. E 60 (2003) 3097.
[28] J. Karger, H. Pfeifer, S. Rudtsch, The influence of internal magnetic field gradients on NMR self-diffusion measurements of molecules absorbed on microporous crystallites, Magn. Reson. Imaging 21 (1989) 193.
[29] Y.Q. Song, L. Venkataramanan, M.D. Hrlimann, M. Flaum, P. Frulla, C. Straley, T1T2 correlation spectra obtained using a fast two-dimensional laplace inversion, J. Magn. Reson. 154 (2002) 261.
[30] M. Winkler, M. Zhou, M. Bernardo, B. Endeward, H. Thomann, Internal magnetic gradient fields in glass bead packs from numerical simulations and constant time diffusion spin echo measurements, Magn. Reson. Imaging 21 (2003) 311.
[31] L. Monteilhet, J.P. Korb, J. Mitchell, P.J. McDonald, Observation of exchange of micropore water in cement pastes by two-dimensional T2–T2 nuclear magnetic resonance relaxometry, Phys. Rev. E 74 (2006) 061404.
[32] P.T. Callaghan, I. Furo, Diffusion–diffusion correlation and exchange as a signature for local order and dynamics, J. Chem. Phys. 120 (2004) 4032.